THE JOURNAL OF BIOLOGICAL CHEMISTRY VOL. 291, NO. 9, pp. 4711–4722, February 26, 2016

Palmitoylation Strengthens Cholesterol-dependent Multimerization and Fusion Activity of Human Cytomegalovirus Glycoprotein B (gB)*

Received for publication, July 31, 2015, and in revised form, December 21, 2015 Published, JBC Papers in Press, December 22, 2015, DOI 10.1074/jbc.M115.682252

Marco Patrone[‡§1], **Ana Sofia Coroadinha**[‡¶], **Ana P. Teixeira**[‡¶], **and Paula M. Alves**[‡¶]

From the [‡]*Animal Cell Technology Unit, iBET Instituto de Biologia Experimental e Tecnológica, 2780-901 Oeiras, Portugal, the* [§]*Biocrystallography Unit, DIBIT Fondazione Centro San Raffaele, 20132 Milano, Italy, and the* [¶]*Instituto de Tecnologia Química e Biológica, Universidade Nova de Lisboa, 2784-505 Oeiras, Portugal*

Herpesviruses are a large order of animal enveloped viruses displaying a virion fusion mechanism of unusual complexity. Their multipartite machinery has a conserved core made of the gH/gL ancillary complexes and the homo-trimeric fusion protein glycoprotein B (gB). Despite its essential role in starting the viral infection, gB interaction with membrane lipids is still poorly understood. Here, evidence is provided demonstrating that human cytomegalovirus (HCMV) gB depends on the *S*-palmitoylation of its endodomain for an efficient interaction with cholesterol-rich membrane patches. We found that, unique among herpesviral gB proteins, the HCMV fusion factor has a Cys residue in the C-terminal region that is palmitoylated and mediates methyl-*β*-cyclodextrin-sensitive self-association of purified gB. A cholesterol-dependent virus-like particle trap assay, based on co-expression of the HIV Gag protein, confirmed that this post-translational modification is functional in the context of cellular membranes. Mutation of the palmitoylated Cys residue to Ala or inhibition of protein palmitoylation decreased HCMV gB export via Gag particles. Moreover, purified gB_{C777A} showed an increased kinetic sensitivity in a cholesterol depletion test, demonstrating that palmitoyl-gB limits outward cholesterol diffusion. Finally, gB palmitoylation was required for full fusogenic activity in human epithelial cells. Altogether, these results uncover the palmitoylation of HCMV gB and its role in gB multimerization and activity.

Human cytomegalovirus (HCMV)[2] belongs to the Herpesviridae sub-family in the Herpesvirales order of enveloped viruses (1). The broad cell tropism and the relapsing life-long infection make this widespread virus associated with a large number of inflammation-related diseases, and a major cause of neuro-developmental disorders as well as of immunosenescence (2–4). Several studies report the remarkable complexity and diversity of the fusion machinery of herpesviruses, required to start the target cell infection. The herpesviral fusion mechanism evolved around two type I integral membrane glycoproteins, the conserved tri-protomeric fusogenic protein gB and the triggering heterodimer gH/gL (5). A number of additional species-specific envelope polypeptides, expressed either as independent transmembrane glycoproteins or as gH/gL complex subunits, complement the two herpesviral core elements providing receptor binding and cell tropism determinants (6–10). HCMV expresses two gH/gL forms, the gO- and the pUL131A-pUL130-pUL128-bearing complexes. The gH pentamer in particular is essential to infect monocytes and endothelial, epithelial, and dendritic cells, as well as for the leukocyte-mediated spread of the infection. The ultimate consequence of the receptor-dependent lateral interactions between the envelope fusion players is the activation of the fusogenic refolding in the gB ectodomain (11, 12). According to the current models of virion-mediated fusion (13), the rearranging gB is supposed to insert two hydrophobic loops per protomer into the target membrane while it folds back and pulls the two membranes close to each other (14–16). This mechanical force is expected to go along with the heat released by the conformational shift, melting and joining together the two bilayers. Hence, the interaction with lipids is central to the activity of viral fusion proteins. Indeed, this is not only limited to membrane joining. For the maturation of the initial outer leaflet splicing (the hemifusion state) into a large pore, the fusion protein units have to multimerize (17, 18). The quantitative rearrangement of virionic gB molecules observed during HCMV entry (11) suggested an uneven distribution of this protein onto the virion surface during the fusion execution. Strikingly, cryo-electron tomography of purified herpes virions has provided strong evidence for post-fusion gB clustering within the viral envelope (19). Although homotypic protein-protein contacts in the gB ectodomain are likely involved, the zonal restraint of gB seen by Grünewald and co-workers (19) in the virion envelope is reminiscent of partitioning within membrane microdomains. Coherently, virionic gB was previously found partially associated to detergent-resistant membranes, whereas cholesterol depletion from purified virions and target cells inhibits the infection (20). Moreover, purified post-fusion full-length

* This work was supported by the European Union (EU) project ComplexINC FP7/2007-2013, Grant 270089 (to P. M. A.) and by Marie Curie Postdoctoral Grant SHerpA FP7-PEOPLE-2009-IEF Grant 251982 and Fundação para a Ciência e a Tecnologia (FCT) Grant EXPL/BBB-BIO/1541/2013 (to M. P.). The authors declare that they have no conflicts of interest with the contents of this article.

[1] To whom correspondence should be addressed: Biocrystallography Unit, Division of Immunology, Transplantation, and Infectious Diseases, DIBIT – San Raffaele Scientific Institute, Via Olgettina 58, 20132 Milano, Italy. Tel.: 39-0226434921; Fax: 39-0226434153; E-mail: patrone.marco@hsr.it.

[2] The abbreviations used are: HCMV, human cytomegalovirus; gB, glycoprotein B; VLP, virus-like particle; MβCD, methyl-β-cyclodextrin; NTA, nanoparticle tracking analysis; rIMP, raft integral membrane proteins; TM, transmembrane domain; IRES, internal ribosomal entry site; DMSO, dimethyl sulfoxide; BN-PAGE, blue native PAGE; Bis-Tris, 2-(bis(2-hydroxyethyl) amino)-2-(hydroxymethyl)propane-1,3-diol; CELISA, cell ELISA.

TABLE 1
Primer list; restriction sites (underlined), start/stop (lowercase) and mutated (boldface) codons, T7 promoter/terminator (italics), and overlapping sequences (underlined boldface) are indicated

Name	Sequence
OFw	5′-TATAAATATAGGATCCCGCCACCatgGAATCCAGGATCTGGTGCCTG-3′
mutFur	5′-GGTGTGAACTCCACGCGT**GCA**ACCAAG**GCT**AGTACGGGCAATACGACCACCCT-3′
C777A	5′-CTATACTCGACAGCGGCGTCTC**GCC**ATGCAGCCGCTGCAAAACCTCTTT-3′
ORv	5′-GCCGCGGTACCTCGAGttaCTTTTCGAATTGCGGATGC-3′
R7BFw	5′-*TAATACGACTCACTATAGGGAGA*atgGAATCCAGGATCTGGTGCCTG-3′
R7BRv	5′-tcaGACGTTCTCTTCTTCGTCAGAG-3′
R7HFw	5′-*TAATACGACTCACTATAGGGAGA*atgCGGCCCGGCCTCCCCTTC-3′
R7HRv	5′-tcaGCATGTCTTGAGCATGCGGTA-3′
R7LFw	5′-*TAATACGACTCACTATAGGGAGA*atgTGCCGCCGCCCGGATTGC-3′
R7LRv	5′-ttaGCGAGCATCCACTGCTTGAGG-3′
R71Fw	5′-*TAATACGACTCACTATAGGGAGA*atgCGGCTGTGTCGGGTGTGGC-3′
R71Rv	5′-ctaGTTGGCAAAGAGCCGCACGC-3′
R70Fw	5′-*TAATACGACTCACTATAGGGAGA*atgCTACGGCTTCTGCTTCGTCAC-3′
R70Rv	5′-tcaAACGATGAGATTGGGATGGGTG-3′
R78Fw	5′-*TAATACGACTCACTATAGGGAGA*atgAGTCCCAAAAACCTGACGCCG-3′
R78Rv	5′-tcaCTGCAGCATATAGCCCATTTTAG-3′
R7T7Fw	5′-*TAATACGACTCACTATAGGGAGA*atgAACACGATTAACATCGCTAAGAAC-3′
R7T7Rv	5′-ttaCGCGAACGCGAAGTCCGACT-3′
D7iLF1	5′-*TAATACGACTCACTATAGGGAGA*GGTACCGCGGGCCCGGGATC-3′
D7iLR1	5′-**CTTCTTAATGTTTTTGGCATCTTCCATTATTATCATCGTGTTTTTCAAAGGAAAAC**-3′
D7iLF2	3′-**GTTTTCCTTTGAAAAACACGATGATAATAATGGAAGATGCCAAAAACATTAAGAAG-3′**
D7iLR2	5′-***AGAGGCCCCAAGGGGTTATGCTA***ttaCACGGCGATCTTGCCGCCCTTCT-*3′*
D7iLR2b	5′-*CAAAAAACCCCTCAAGACCCGTTT**AGAGGCCCCAAGGGGTTATGCTA***-3′

HCMV gB stably associates with host cell-derived lipids (21). In the present work, the gB-lipid relationship has been investigated and the *S*-palmitoylation of HCMV gB endodomain is reported. A virus-like particle (VLP)-based assay showed that palmitoylation modulates gB targeting to cholesterol-rich membrane domains. Furthermore, acylation was responsible for the stable coalescence of purified gB bicelles in a cholesterol-dependent fashion. Finally, palmitoylation affected gB cell surface expression and strongly contributes to gB fusion activity. The sequence comparison of gB protein homologs indicates that acylation is a distinctive feature of HCMV gB. Hypotheses on the virion-mediated fusion mechanism and for synthetic vaccine design are discussed.

Experimental Procedures

Primary Antibodies—Antibodies used were: anti-p24 (mAb HIV anti-p24 clone 39/5.4A, Abcam); anti-gB (mAb clone 2F12, Abcam); anti-biotin (mAb clone DVP.6, Creative Diagnostics); rabbit polyclonal anti-flotillin 1 (Abcam, catalog number ab41927); anti-transferrin receptor (mAb clone H68.4, Thermo Scientific); and anti-α1 Na^+/K^+ ATPase antibody (mAb clone 464.6, Abcam).

Cell Lines—High Five™ cells were maintained in Insect-XPRESS™ medium (Lonza) supplemented with 0.5 mM *N*-acetyl-L-cysteine (Sigma-Aldrich) in a shaking incubator at 27 °C. ARPE19 cells (ATCC® CRL-2302™) were grown in DMEM supplemented with 10% FBS, 1× antibiotic/antimycotic (Gibco, Life Technologies), and 0.5 mM *N*-acetyl-L-cysteine.

Mutagenesis, Expression, and Purification of gB Protein Variants—All of the PCR and cloning reactions were carried out with Phusion® DNA polymerase (Thermo Scientific) and In-Fusion® enzyme (Clontech), respectively. The primers used are listed in Table 1. Full-length HCMV UL55 ORF strain VR1814 with a Twin-Strep-tag™ (21) and with the dispensable Furin site ablated (*i.e.* changing Arg-456/459 to Ala; primer mutFur) was used as a wild type reference. C777A mutation was introduced to generate gB_{C777A}-coding ORF. The recombinant ORFs were inserted into the pOET1 transfer vector (primers OFw and ORv), sequence was validated, and recombinant baculovirus vectors were generated with *flash*BACGOLD (Oxford Expression Technologies) following the manufacturer's guidelines. Recombinant gB proteins were expressed and purified as already described (21) with some modifications. Briefly, infections of High Five™ cells were performed in Optimum Growth™ 5-liter flasks (Thomson Instrument Company). Glucose and glutamine were kept at 30 and 7 mM, respectively. gB protein variants were purified onto a 5-ml Strep-Tactin® HP column (GE Healthcare), omitting the use of dithiothreitol. Resin bound-proteins were extensively washed with 10 mM methyl-β-cyclodextrin (MβCD, Sigma-Aldrich) before elution. gB and gB_{C777A} proteins were obtained as spontaneously formed 600-kDa bicelles, containing host-cell lipid carry-over as reported previously (21). Final yields were 0.8 mg/liter for either gB or gB_{C777A}; both proteins were stored in 100 mM Tris·HCl, 0.15 mM NaCl, 0.05% w/v cymal-5 (Anatrace), 20% v/v glycerol, pH 8 (protein buffer).

VLP Production and Quantification—A recombinant baculovirus vector encoding the HIV $Pr55^{Gag}$ was generated as described above, with the DNA encoding HIV $Pr55^{Gag}$ transferred from pMDLg/pRRE (22). $Pr55^{Gag}$ was co-expressed with either gB or gB_{C777A} by co-infecting High Five™ cells at 10^6 cell/ml with three plaque-forming units/cell of each baculovirus derivative. For cholesterol depletion/repletion experiments, cells at 45 h after infection were incubated 45 min with or without 10 mM MβCD. MβCD wash-out was followed by a 2-h incubation in medium supplemented with 0.3 mM cholesterol (Sigma-Aldrich) or vehicle alone (0.1% DMSO, 0.01% chloroform). In some experiments, cells were incubated for 18 h in culture medium containing 50 μM 2Br-palmitate (Sigma-Aldrich). VLPs were harvested from ≥95% viable cell culture supernatants as described elsewhere (23). In brief, cell culture supernatants were 0.45-μm-filtered and centrifuged at 125,000 × *g* for 1 h. The pellet was resuspended, loaded over a 20% sucrose cushion, and centrifuged at 200,000 × *g* for 1.5 h.

Final pellets were measured by nanoparticle tracking analysis (NTA) with NS500 (NanoSight, Malvern Instruments), and corresponding VLP titers were obtained (all the quantifications reported in this study are expressed as mean ± S.D., $n = 3$). Collected samples were also probed in immunoblots for $Pr55^{Gag}$ or gB.

Acyl-Biotinyl Exchange—An acyl-Biotinyl exchange assay (24) was performed according to Brigidi and Bamji (25) and adapted to Strep-Tactin chromatography. In brief, insect cells expressing gB or gB_{C777A} were washed and lysed in the presence of 20 mM Tris[2-carboxyethyl]phosphine hydrochloride and 50 mM *N*-ethylmaleimide (both from Sigma-Aldrich) to quench unmodified cysteine residues. Clarified cell lysates were incubated with Strep-Tactin resin using an Amicon® Pro purification device with a 100-kDa nominal molecular weight cut-off filter (Merck Millipore). The acyl-biotin exchange was initiated by washing the resin with 0.5 M hydroxylamine. Acylated Cys residues were labeled with 1 μM BMCC-biotin (Pierce) in the elution buffer containing 2.5 mM biotin. Eluted and concentrated material were revealed by immunoblot with mAbs anti-gB or anti-biotin.

PCR Constructs, in Vitro mRNA Synthesis, and Transfections—HCMV gH, gL, pUL130, pUL131A, and pUL128 (6) as well as tag-less gB and gB_{C777A} open reading frames were amplified with RT7-H, -L, -0, -1, -8, and -B primer pairs, respectively (Table 1). T7 RNA polymerase coding sequence was amplified from *Escherichia coli* BL21(DE3) genomic DNA with R7T7Fw/Rv primer pair. All the above PCR products possessed a T7 promoter sequence at their 5′ end.

IRES sequence was amplified from pIRES2-EGFP vector (Clontech) with D7iLF1/D7iLR1 primer pair. The resulting amplimer was PCR-spliced with firefly luciferase cDNA, the latter amplified from pGL4 vector (Promega) using the D7iLF2/D7iLR2 primers and further extended at the 3′ end with the D7iLR2b primer. The resulting p7IRESLuc hybrid DNA molecule had the T7 promoter and terminator sequences to the 5′ and 3′ end of a IRES-luciferase transcription unit, respectively.

Capped and polyadenylated mRNAs for gB variants, gH pentamer sub-units, and T7 RNA polymerase were individually synthesized from the respective PCR products with the mMESSAGE mMACHINE® T7 Ultra Kit (Ambion, Life Technologies) and purified according to the manufacturer's instructions. Each transcription product was individually complexed with the transfection vehicle for RNA cell transfection (*Trans*IT®-mRNA Transfection Kit, Mirus Bio), and mRNA-vehicle complexes were mixed afterward to give the combinations described under "Results" (we found this is to be a more efficient procedure for co-transfections). DNA transfection of p7IRESLuc PCR product was with FuGENE® HD (Promega). In all of the experiments, mock transfections were performed for baseline correction.

Detergent-free Raft Flotation—The method developed by Persaud-Sawin *et al.* (26) was used. Briefly, 10^8 ARPE cells were mRNA-transfected in culture medium containing 10% dialyzed FBS to express either gB or gB_{C777A}. Cells were harvested 18 h after transfection and lysed at 4 °C in a Dounce homogenizer in 250 mM sucrose, 20 mM Tris·HCl, 1 mM $CaCl_2$, 1 mM $MgCl_2$, cOmplete protease inhibitor cocktail (Roche Applied Science), pH 8. The post-nuclear supernatant was mixed 1:1 (v/v) with the lysis buffer containing 85% sucrose, placed at the bottom of ultracentrifuge tubes, and overlaid with 35% and then 5% sucrose in the same buffer. Samples were centrifuged at 200,000 × *g* for 18 h at 4 °C. Fractions were collected from the bottom and probed in immunoblot for gB, flotillin 1, and the transferrin receptor. In some experiments, cells were cholesterol-depleted with 10 mM MβCD or incubated with 50 μM 2Br-palmitate as described above.

Analysis of gB Multimerization and Competition Dialysis—gB multimerization was induced by mixing purified gB or gB_{C777A}, obtained in their spontaneous 600-kDa form, with 50 μM cholesterol dissolved into the protein buffer for 1 h at 37 °C, without further manipulations. Multimers were visualized by blue native protein electrophoresis (BN-PAGE) in a 4–16% NativePAGE™ Novex® Bis-Tris pre-cast gel system (Life Technologies) and analyzed in a ChemiDoc XRS+ with Quantity One® 1-D analysis software (Bio-Rad) within the 0.5–5-μg linear range. gB monomers were quantified against cholesterol-free gB. Results were expressed as monomer fractional abundance and fitted with a regression analysis (GraphPad Prism 6.0, GraphPad Software).

For multimer dissociation experiments, 100 μl of either gB or gB_{C777A} cholesterol-induced multimers were loaded into a 2-kDa nominal molecular weight cut-off micro-dialysis device (Pierce, Thermo Scientific). The dissociation was started by placing the sample at 37 °C against a reservoir of identical volume filled with buffer containing equimolar cymal-5:MβCD concentrations as follows. For the steady-state equilibrium dialysis, each gB variant (1.7 μM final concentration) was incubated for 1 h with the indicated MβCD concentrations in the reservoir. For the time-course analysis, 1.7 μM gB or gB_{C777A} was incubated with 10 mM MβCD in the dialysis reservoir, and the protein was sampled at increasing time points. The samples were analyzed by BN-PAGE and densitometry as above.

Analysis of gB Surface Expression—ARPE cells that were mock, gB, or gB_{C777A} mRNA-transfected as above were processed 18 h after transfection for CELISA (procedure described in Ref. 11), and steady-state surface expression was measured with 2F12 mAb.

gB surface dynamic trafficking was measured 16 h after mRNA transfection by incubating ARPE cells in 50 mM NH_4Cl- and 2F12 mAb-containing medium for 30 min. Then cells were washed and lysed in 1% Triton X-100 PBS, and clarified cell lysate was loaded into polystyrene microplates (Nunc MaxiSorp®, Thermo Scientific). Internalized anti-gB antibody was quantified in ELISA with anti-mouse horseradish peroxidase conjugate and *o*-phenylenediamine dihydrochloride (Sigma). Some experiments were performed in the presence of 2Br-palmitate as above. Values were plotted after mock signal subtraction.

Flow cytometry on mock, gB, or gB_{C777A} mRNA-transfected ARPE cells was performed 16 h after transfection. Cells were detached by using TrypLE™ Select (10×) reagent (Thermo Scientific), washed in cold 1× Dulbecco's PBS, 0.5 mM EDTA, and resuspended in cold 3% formaldehyde at 10^5 cells/ml under continuous agitation. Cells were labeled without permeabiliza-

tion with mAb 2F12, stained with R-phycoerythrin-CF594-conjugate anti-mouse (BD Biosciences), and analyzed in a BD FACSCanto™ II (BD Biosciences). Plasma membrane protein fractionation from gB or gB_{C777A} transfectant ARPE cells was performed according to Schindler and Nothwang (27) and used the plasma membrane protein extraction kit (Abcam), following the manufacturer's instructions.

Fusion Assay in Human Epithelial Cells—Parallel ARPE monolayers were transfected with gB or gB_{C777A}, gH pentamer, and T7 RNA polymerase mRNAs (donor cells) or with p7IRESLuc (target cells). After 6 h, cells were extensively washed with culture medium containing 50 μg/ml heparin to stop the transfection. Target transfectants were then co-seeded 1:3 with donor cells and incubated for an additional 12 h. In some experiments, the fusion assay was performed in the presence of 50 μM 2Br-palmitate and 10% dialyzed FBS. Luciferase activity (Luciferase Assay System, Promega) was then quantified in a plate luminometer (Clarity™, BioTek). To visualize cell syncytia, ARPE cells were mRNA-transfected as for the donor cells above, stained supravitally with DAPI and imaged under an inverted microscope (Axio Observer, equipped with an AxioCam MRm CCD camera, Zeiss).

Results

The recombinant 360-kDa tri-protomeric gB was previously reported to carry over lipids from host cells, forming a spontaneous bicelle of ~600 kDa (hereafter referred to as gB monomer) when purified under reducing conditions (21).

gB Associates with Rafts at the Plasma Membrane—To investigate whether the lipid domain surrounding gB was derived from membrane microdomains, and to study gB targeting to cholesterol-rich microdomains, a VLP-based assay was set up in insect cells. The HIV capsid assembles at plasma membrane lipid rafts (28), sampling and exporting raft-associated proteins during budding. At the same time, distantly related insect host cells allow us to focus on autonomous gB targeting elements, conserving the post-translational modifications.

In baculovirus-infected insect cells, $Pr55^{Gag}$ is released as pleomorphic immature particles in a protease- and Rev-independent manner (29). The diameter of the particles obtained ranged between 150 and 250 nm, with a peak at 200 nm (Fig. 1*A*). The comparison with the control from $Pr55^{Gag}$-negative infected cells showed that contamination by *Autographa californica* multicapsid nucleopolyhedrovirus (*Ac*MNPV) virions or structured cell debris was undetectable from samples collected at ≥90% cell viability (detection limit 10^6 particles/ml). Co-expressed gB co-sedimented with $Pr55^{Gag}$ VLPs (Fig. 1*B*). A faint gB signal was present in the $Pr55^{Gag}$-negative control, likely due to a low degree of cell lysis or exosome secretion. Sterol depletion/repletion tests verified that Gag-mediated gB export was cholesterol-dependent (Fig. 2). Subtraction of sterols by 10 mM MβCD effectively inhibited $Pr55^{Gag}$ particle release by ~85% (from 3.2 ± 1.8 to $0.54 \pm 0.23 \times 10^{11}$ particles/liter^{-1} in control *versus* sterol-depleted cultures, Fig. 2*A*). Supplementing stripped cells with exogenous cholesterol partially restored $Pr55^{Gag}$ VLP concentration ($1.9 \pm 1.2 \times 10^{11}$ particles/liter^{-1}). gB export displayed the same trend, with a significant reduction of its abundance in the supernatants from

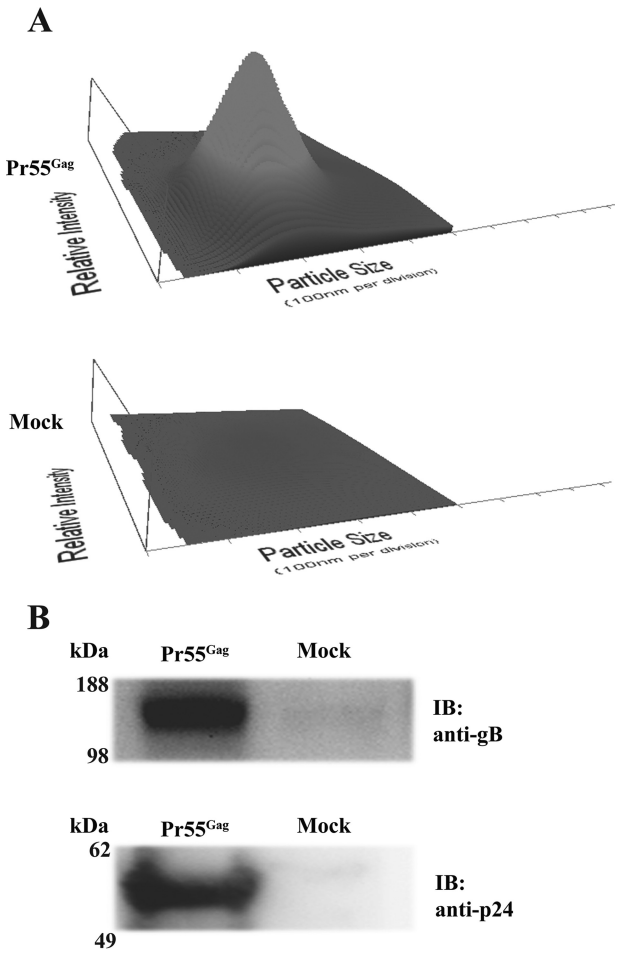

FIGURE 1. **HCMV gB co-fractionates with $Pr55^{Gag}$ VLPs.** *A*, NTA of the particles recovered from culture medium of co-infected cells expressing gB with (*$Pr55^{Gag}$*) or without (*Mock*) HIV $Pr55^{Gag}$, following the protocol described under "Experimental Procedures." Plots showing particle size (nm, on *x* axis), scattered light intensity (relative units, *y* axis), and concentration (10^6/ml, z direction) were generated with NanoSight NTA 2.3 software (NanoSight, Malvern Instruments). The parental *Ac*MNPV vector replaced $Pr55^{Gag}$-expressing baculovirus in co-infections of mock controls. *B*, immunoblot (*IB*) with anti-gB or -p24 antibody on the VLP fraction and mock control shown in *A*; the same volume of each preparation was loaded for blotting.

MβCD-treated cells that could be amended by back-supplementation of cholesterol (Fig. 2*B*). Incorporation into $Pr55^{Gag}$ VLPs is, then, a consistent assay for evaluating raft association of membrane proteins. Notably, the extent of the MβCD effect suggested that membrane microdomains influence gB residence time on the cell surface. On the other hand, comparing VLP titers with immunoblot signals (Fig. 2, *A* and *B*) suggests that cholesterol repletion shock caused the release of particles barely resistant to the VLP harvesting procedure. Indeed, $Pr55^{Gag}$ immunoblot signals did not reflect the particle titers recorded by NTA, the latter having a 30 nm detection limit and possibly unable to sense fragmented particles.

Palmitoylation of gB Endodomain—HCMV gB has a single Cys residue in the endodomain (Cys-777), close to an Arg-rich stretch featuring the juxtamembrane region of this protein (Fig. 3*A*). Hence, Cys-777 resembles the transmembrane proximal palmitoylation sites found in other fusion proteins from unre-

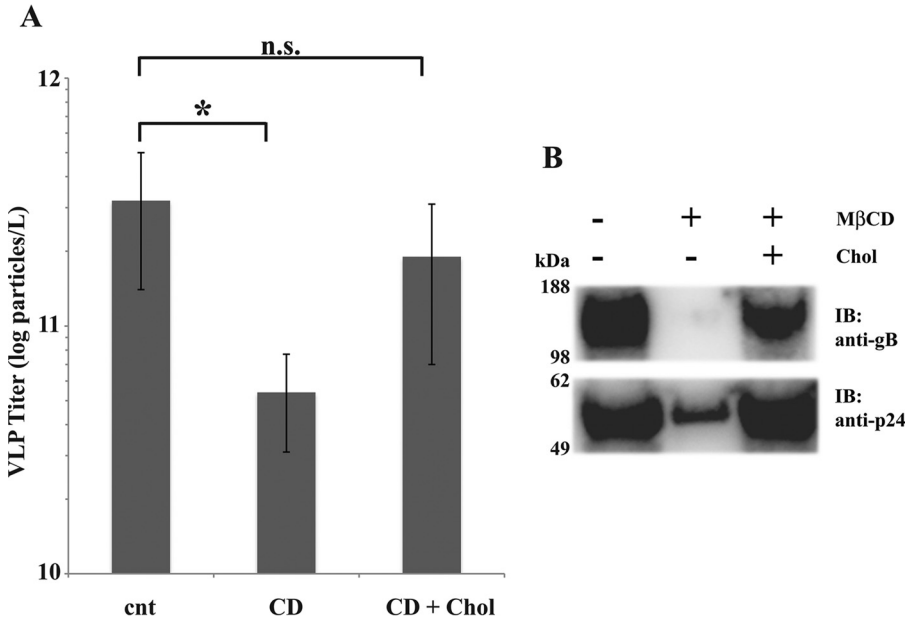

FIGURE 2. **Pr55^{Gag} VLP production and gB export have similar sensitivity to cholesterol depletion.** *A* and *B*, VLP titers (*A*) and anti-gB or -p24 immunoblot (*IB*) (*B*) on VLP fraction collected (as in Fig. 1) from cells treated or not with 10 mM MβCD, with or without cholesterol repletion. After MβCD or mock wash-out, cell cultures were incubated in culture medium containing 0.1% DMSO, 0.01% chloroform with or without 0.3 mM cholesterol (*Chol*). Equal loading was as in Fig. 1*B*. Abbreviations in *A*: *cnt*, vehicle control; *CD*, MβCD; *CD + Chol*, cholesterol repletion. *Error bars* indicate mean ± S.D. *, *p* value ≤ 0.05, *n. s.*: not significant; statistical analysis was conducted with two-tailed *t* test.

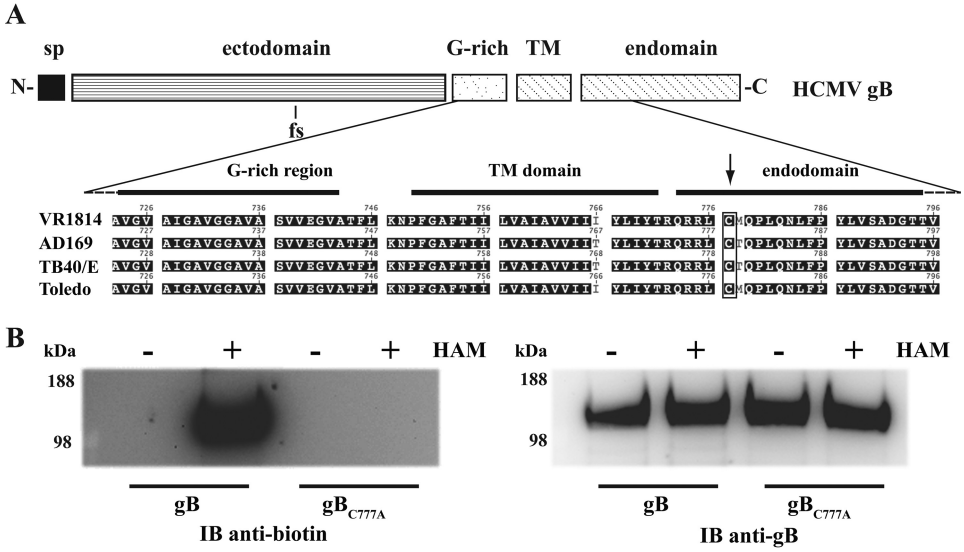

FIGURE 3. **gB endodomain harbors a palmitoylated cysteine residue.** *A*, schematic diagram of HCMV gB protomer (*sp*, signal peptide; *TM*, transmembrane helix). The close-up shows the juxtamembrane and TM amino acid sequence alignment from different HCMV strains (see Footnote 3) with the endodomain Cys residue highlighted; due to two polymorphic sites in the gB ectodomain, residue numbering differs slightly among the four strains. The Cys-777 position number refers to the VR1814 gB allele used in this study. *B*, acyl-biotinyl exchange assay on purified gB and gB$_{C777A}$ as described under "Experimental Procedures." Hydroxylamine (*HAM*) was omitted in a series of samples as a control. Eluted proteins were probed in immunoblot (*IB*) with anti-biotin to detect labeled Cys residues or anti-gB antibody to verify the equal loading.

lated enveloped viruses (30).[3] In an acyl-biotin exchange assay, gB was labeled with BMCC-biotin specifically after thioester bond cleavage with hydroxylamine (Fig. 3*B*). Replacing Cys-777 with an Ala residue abolished gB thio-biotinylation, demonstrating that the HCMV gB endodomain actually undergoes *S*-palmitoylation.

Palmitoylation does not necessarily correlate to protein localization into membrane microdomains (31), although palmitoylation dominates among raft proteins (32). Indeed, *S*-acylation turned out to enhance gB sorting with cholesterol-rich microdomains (Fig. 4). Although the intracellular levels were similar to those of parental gB (Fig. 4*A*), the gB$_{C777A}$ mutant was inefficiently exported in the VLP trap assay (Fig. 4*B*). Nevertheless, gB$_{C777A}$ export was also sensitive to sterol

[3] GenBank™ accession numbers: HCMV strains GU179289 (VR1814), X17403 (AD169), EF999921 (TB40/E) and GU937742 (Toledo); HSV-1 JQ673480; VZV NC 001348; EBV NC 007605; HHV-6A NC 001664; HHV-7 NC 001716; and KSHV NC 009333. Abbreviations used in this footnote are: VZV, varicella zoster virus; HHV-6A, human herpesvirus 6A; HHV-7, human herpesvirus 7; KSHV, Kaposi's sarcoma-associated herpesvirus.

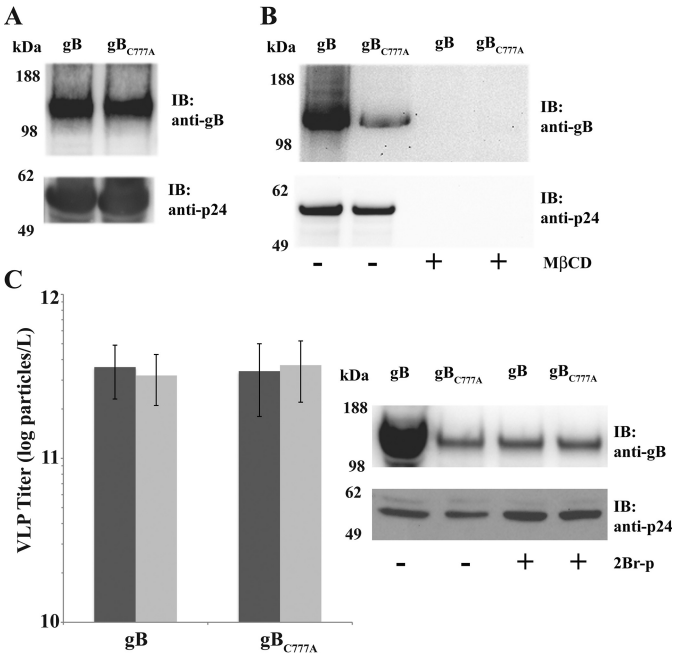

FIGURE 4. **Palmitoylation is required for efficient HCMV gB targeting to Pr55^{Gag} VLPs.** *A*, anti-gB and -p24 immunoblots (*IB*) on total cell extracts from cells expressing Pr55^{Gag} together with gB or gB$_{C777A}$. For all samples, 10^5 cell equivalents were loaded for blotting. *B*, immunoblot on VLP fractions obtained from cell cultures in *A* after mock or MβCD treatment and wash-out. Equal loading was as in Fig. 1*B*. *C*, particle titers (*left panel*) and anti-gB or -p24 immunoblots (*right panel*) on Pr55^{Gag} VLPs from cells co-expressing gB or gB$_{C777A}$ treated or mock-treated (*dark gray* and *light gray* in the *left panel*, respectively) with 50 μM 2Br-palmitate (*2Br-p*). Equal loading was as above. *Error bars* indicate mean ± S.D.

depletion by MβCD. Inhibition of protein-acyl transferases with 2Br-palmitate confirmed that gB raft association was enhanced by *S*-acylation (Fig. 4*C*). VLPs produced from cells incubated with the palmitoylation inhibitor contained a very low amount of gB, whereas neither incorporation of gB$_{C777A}$ nor Pr55^{Gag} export was substantially affected.

gB partition into lipid rafts was confirmed in flotation tests on extracts from mRNA-transfected human epithelial cells (Fig. 5; see also "Experimental Procedures"). gB was present in the fractions positive for human flotillin 1, whereas most of the gB$_{C777A}$ co-migrated with the non-raft marker transferrin receptor. gB variants were absent in the top gradient fractions of the extracts from cells treated with MβCD, whereas 2Br-palmitate reduced the amount of gB associated with rafts.

Both VLP trap and flotation assays showed that palmitoylation increases gB basal association with cholesterol-rich membrane domains, although none of the above approaches distinguish interaction strength from kinetic effects. Taking advantage of purified full-length HCMV gB (21), we further analyzed the influence of palmitoylation on the gB-cholesterol relationship.

Palmitoyl-gB Forms Stable Cholesterol-dependent Multimers—Both gB and gB$_{C777A}$ recombinant variants were obtained at homogeneity with similar yields, confirming that C777A mutation does not affect gB stability (Fig. 6*A*; see also "Experimental Procedures"). To preserve palmitoylation, the use of dithiothreitol was omitted and monomeric gB was obtained by stripping host cell sterols in the chromatographic steps. As expected from previous observations (21), gB$_{C777A}$ was found embedded in a particle of the same size as the wild type protein (Fig. 6*B*). More interestingly, cholesterol subtraction did not affect the integrity of the bicelle surrounding gB, proving that neither cholesterol nor palmitoylation is required for gB monomer embedding. At the same time, palmitoylation does not confer generic stickiness to gB. The effect of cholesterol on gB was evaluated in a 2-fold dilution series of either wild type gB or the C777A mutant in protein buffer containing a final concentration of 50 μM cholesterol. In this way, the same cholesterol:detergent equilibria were kept across the series. Cholesterol consistently triggered gB oligomerization at different molar ratios, with 2- and 3-fold gB multimers visible in BN-PAGE but undetectable gB monomers (Fig. 6*C*). Conversely, non-palmitoylated gB$_{C777A}$ displayed a weaker response to cholesterol, with ~25% of the protein remaining in the monomeric form (0.23 ± 0.02 monomer fractional abundance). For both wild type and the C777A mutant gB, protein dilution and increasing cholesterol:protein molar ratio compensated for each other, ruling out that multimerization was merely due to a solvent effect.

Palmitoylation Reduces Cholesterol Diffusion from gB Multimers—gB-cholesterol interaction was analyzed by competition dialysis (see "Experimental Procedures"). Differential sensitivity to MβCD of cholesterol-induced multimers with purified gB and gB$_{C777A}$ showed that the palmitoyl moiety increases gB clustering by stabilizing cholesterol-dependent coalescence (Fig. 7). In standard competition dialysis experiments, MβCD reverted cholesterol-induced gB association in a dose-dependent manner after a 1-h incubation (Fig. 7*A*), although a low amount of oligomeric gB was still present at the highest MβCD concentration. However, gB and gB$_{C777A}$ displayed similar sensitivity at the steady state with 4.2 ± 0.012 and 2.5 ± 0.015 mM MβCD EC$_{50}$, respectively. This finding argues against a role of palmitoyl-Cys-777 in putative cholesterol binding sites within the gB transmembrane domain. By contrast, a clear difference for multimer dissociation was detected at a kinetic level (Fig. 7*B*). When incubated with 10 mM MβCD, gB$_{C777A}$ multimeric forms exhibited a fast decay curve, whereas gB dissociation followed a sigmoidal trend with a 6-fold longer multimer half-life ($t_{½}$ 3.9 ± 1.2 and 22.2 ± 0.3 min for gB$_{C777A}$ and gB, respectively).

In agreement with VLP trap and raft flotation experiments, multimerization tests confirmed that palmitoylation enhances the basal gB responsiveness to cholesterol. The steady-state and kinetic analyses jointly provide the evidence that diffusion of cholesterol out of the purified gB multimers was limited by the presence of the palmitoyl-Cys residue. In turn, the stiffness of such a milieu seems sufficient to prevent palmitoyl-gB multimers from splitting into monomers, as shown by the palmitoylation-dependent high tendency of gB to stay clustered in the presence of cholesterol.

Efficient gB Fusion Activity Requires Endodomain Palmitoylation—The observations collected pointed out that cholesterol- and acylation-dependent multimerization reflects the strength of raft association around the HCMV fusion factor. Measuring gB-mediated membrane fusion in HCMV-permissive epithelial cells highlighted that gB endodomain palmitoy-

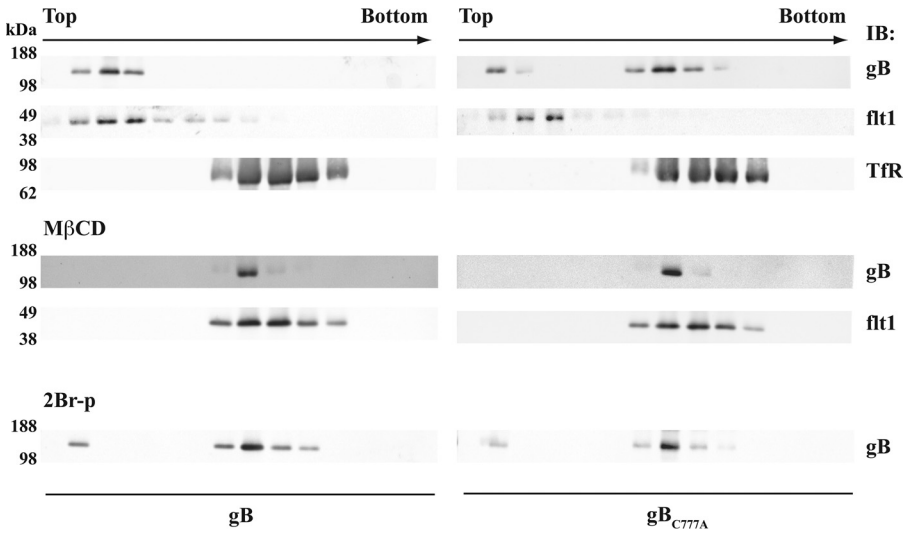

FIGURE 5. **Palmitoylation-dependent gB partition with lipid rafts in human cells.** ARPE cells were transfected with mRNAs coding for gB or gB$_{C777A}$ and processed for raft flotation as described under "Experimental Procedures." After ultracentrifugation, the density gradients were collected in 850-μl fractions, and the first 12 from the tube top were probed in immunoblot (*IB*) for gB, flotillin 1 (*flt1*), or the transferrin receptor (*TfR*). Cells were cholesterol-depleted with 10 mM MβCD (*middle panel*) or incubated with 50 μM 2Br-p (*lower panel*) as described in the legend for Fig. 4. Equal loading was as above.

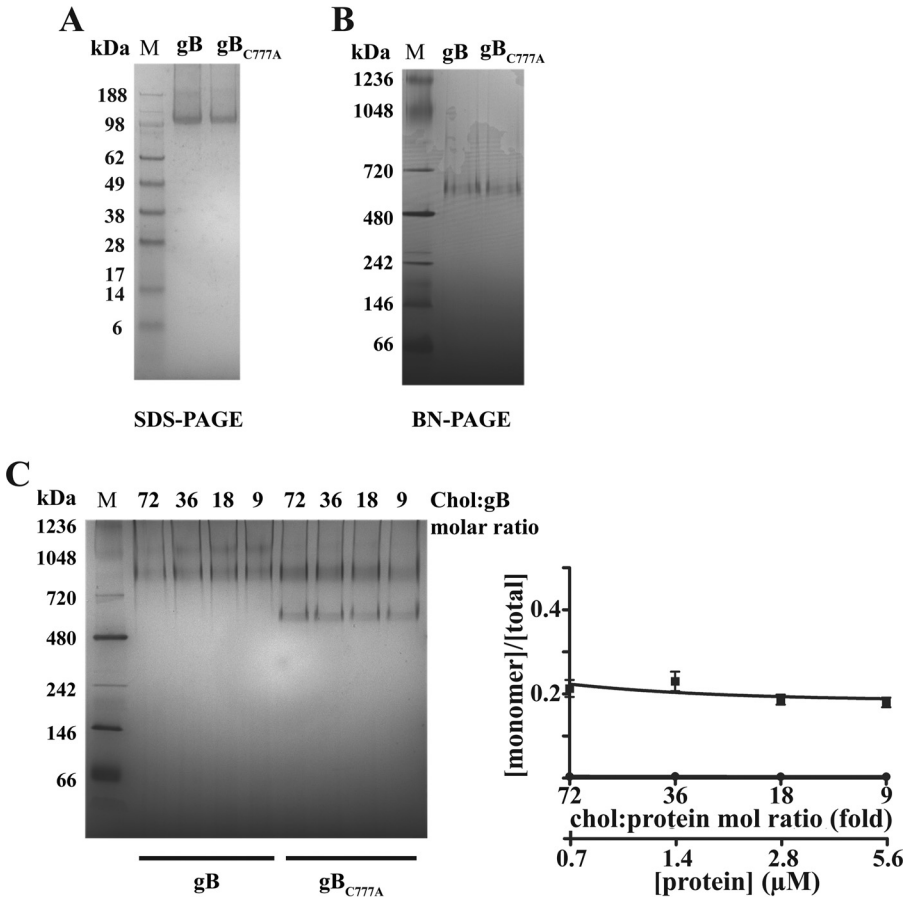

FIGURE 6. **Cholesterol-induced multimerization of purified full-length gB.** *A* and *B*, denaturing (*A*) and native (*B*) gel electrophoresis of purified gB and gB$_{C777A}$ proteins (*M*, molecular weight markers). *C*, *left panel*, purified gB and gB$_{C777A}$ were incubated with 50 μM cholesterol (*Chol:gB*) at the indicated molar ratios (*chol:protein mol ratio*) and protein concentrations for 1 h at 37 °C in 20-μl final volumes, as described under "Experimental Procedures." 5 μg of each protein sample were visualized by BN-PAGE. *Right panel*, BN-PAGE densitometry (*circles*, gB; *squares*, gBC777A). *Error bars* indicate mean ± S.D.

lation is also required for full gB activity (Fig. 8) The functional influence of palmitoylation on gB-mediated fusion was evaluated in a luciferase reporter assay, using RNA transfections. This experimental setup avoids membrane saturation and may better approximate the temporary nature of the virion-target cell interaction.

As for insect cells, gB and gB$_{C777A}$ had similar intracellular expression levels, with the palmitoylation-deficient gB$_{C777A}$

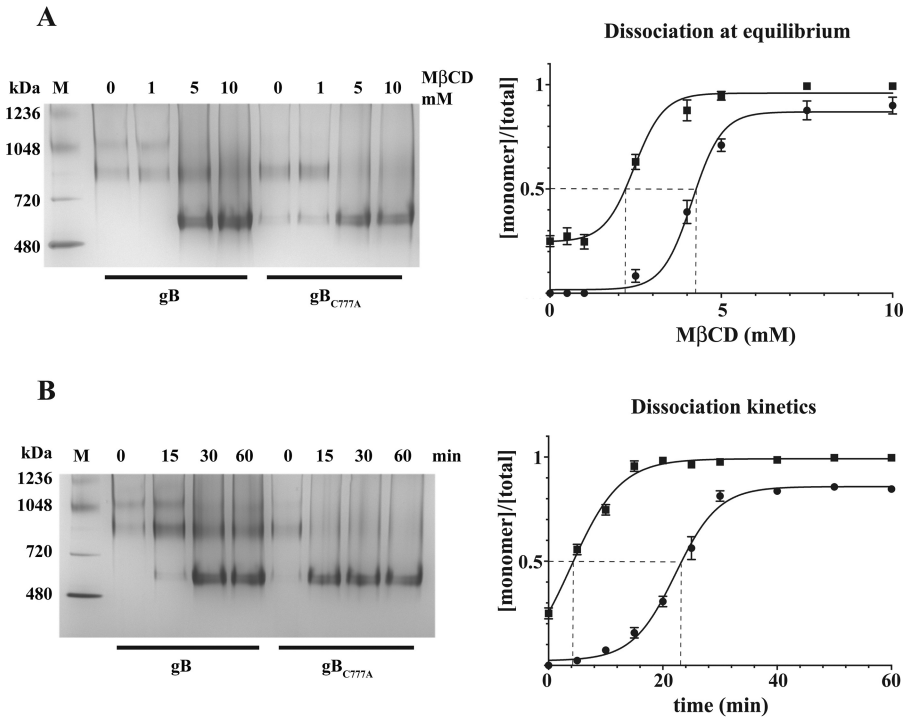

FIGURE 7. **Sensitivity to cholesterol subtraction by gB and gB_{C777A} multimers.** *A*, *left panel*, 5 μg of cholesterol-induced multimers of gB or gB_{C777A} were subject to equilibrium competition dialysis with the indicated MβCD concentrations as described under "Experimental Procedures" and visualized by BN-PAGE (*left panel*). (*M*, molecular weight markers). *Right panel*, densitometric analysis was plotted, and MβCD EC_{50} (*dashed lines*) was calculated with GraphPad Prism 6.0 (*circles*, gB; *squares*, gB_{C777A}). *Error bars* indicate mean ± S.D. *B*, gB and gB_{C777A} multimers were incubated for competition dialysis with 10 mM MβCD and sampled at the indicated time points. The reactions were visualized, quantified, and plotted as in *A* to calculate multimer half-life (*dashed lines*). *Error bars* indicate mean ± S.D.

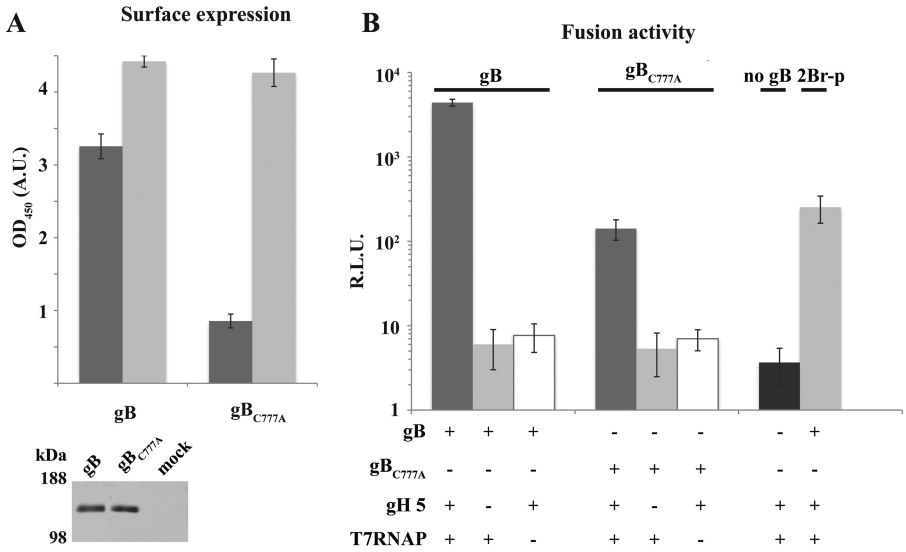

FIGURE 8. **Palmitoylation dependence of gB surface expression and fusion activity in human endothelial ARPE cells.** *A*, plasma membrane steady-state expression (*dark gray*) and dynamic trafficking (*light gray*) of gB or gB_{C777A} expressed by mRNA transfection in ARPE cells were measured by CELISA as described under "Experimental Procedures." *Error bars* indicate mean ± S.D. *Lower panel*, anti-gB immunoblot on transfected ARPE total cell extracts. *OD*, optical density; *A. U.*, absorbance units. *B*, gB or gB_{C777A} mRNA was co-transfected with or without mRNAs coding for gH pentamer subunits (*gH 5*) and T7 RNA polymerase (*T7RNAP*) into ARPE cells and then mixed with cells transfected with p7IRESLuc DNA (see "Experimental Procedures"). gH 5- and T7RNAP-positive, gB-negative transfections were used as control. In one experimental group, the fusion assay was carried out in the presence of 50 μM 2Br-palmitate (*2Br-p*). Luciferase activity was recorded and plotted after subtracting mock transfection signals. *Error bars* indicate mean ± S.D.

mutant showing a 4-fold reduction at the plasma membrane of ARPE cells (Fig. 8*A*). The lower steady-state surface abundance was not due to defective gB_{C777A} targeting. An anti-gB antibody was equally captured by cells expressing either wild type gB or the C777A mutant, demonstrating that similar protein amounts reached the plasma membrane. Along with the VLP trapping in insect cells, the latter result demonstrated that thioacylation affects cell surface gB residence time independently of the cell origin.

Fusion activity was quantified in a well established reporter assay. The assay is based on the cytoplasmic transcription by T7 RNA polymerase of a reporter transcription unit in target

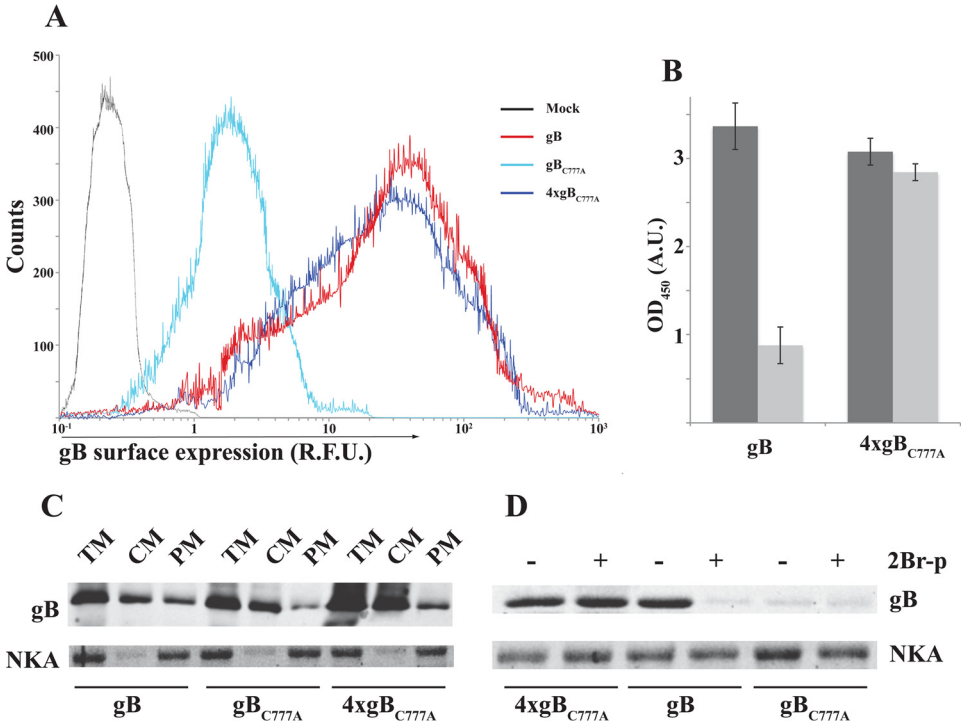

FIGURE 9. **Palmitoylation is not essential for gB targeting to the plasma membrane.** *A*, ARPE cells were transfected with the indicated relative amounts of gB- or gB$_{C777A}$-coding mRNAs, and gB surface expression was analyzed by flow cytometry as described under "Experimental Procedures." The data show an mRNA transfection efficiency ≥90%. *R. F. U.*, relative fluorescence units. *B*, gB surface expression was quantified by CELISA (see "Experimental Procedures") as in *panel A* in the presence (*light gray*) or absence (*dark gray*) of 50 μM 2Br-palmitate (*2Br-p*). *Error bars* indicate mean ± S.D. *OD*, optical density; *A. U.*, absorbance units. *C*, transfected ARPE cell extracts were fractionated by the two-phase method (see "Experimental Procedures"), and partition of gB or gB$_{C777A}$ between total cell membranes (*TM*), cytoplasmic membranes (*CM*), and plasma membrane (*PM*) was analyzed in immunoblots loaded with 10 μg of total proteins and compared with the plasma membrane marker α1 Na^+/K^+ ATPase (*NKA*). *D*, 60 μg of total proteins of plasma membrane fractions from ARPE cells transfected and processed as in *C*, with or without prior incubation in 50 μM 2Br-palmitate (*2Br-p*), were probed in immunoblot for gB or α1 Na^+/K^+ ATPase.

transfectants, when membrane fusion takes place with polymerase donor cells. Luciferase activity was consistently above T7RNAP-negative control in a gB and gH pentamer-dependent manner (Fig. 8*B*). Importantly, the reporter signal was substantially lower when gB$_{C777A}$ replaced wild type gB as the fusion factor or in the presence of 2Br-palmitate; hence the assay output was sensitive to the level of gB surface expression and protein palmitoylation. Nevertheless, the extent of reduction was larger than the gB$_{C777A}$ deficit at the plasma membrane.

Palmitoylation turned out not to be a primary signal for targeting gB to the plasma membrane (Fig. 9). Flow cytometry, CELISA, and two-phase plasma membrane protein fractionation consistently showed that gB$_{C777A}$ is not prevented from reaching the cell surface. Actually, gB$_{C777A}$ expression at the cell surface was increased by transfecting four times the amount of the corresponding mRNA relative to the wild type protein. Moreover, the increase in the plasma membrane levels obtained by overexpressing gB$_{C777A}$ was poorly sensitive to the palmitoylation inhibitor (Fig. 9, *B* and *D*). Normalized cell surface expression showed a substantial dependence on *S*-palmitoylation by the gB ability to promote membrane fusion (Fig. 10). In fact, use of both 2Br-palmitate and gB$_{C777A}$ resulted in about 80% reduction of the luciferase signal (Fig. 10*A*). The fusion defect in the palmitoylation-deficient gB$_{C777A}$ mutant was also detectable as a reduced syncytiogenic ability with respect to wild type gB in transfected cells (Fig. 10*B*). Co-transfecting ARPE cells with gB and gH pentamer mRNAs resulted in the formation of large multinucleated cells made of several nuclei, whereas replacing gB with gB$_{C777A}$ led to smaller syncytia with few nuclei.

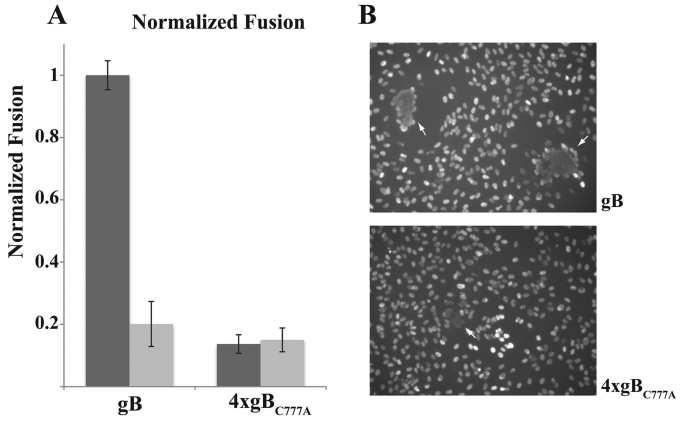

FIGURE 10. **Palmitoylation is required for full gB fusion activity.** *A*, ARPE cells were transfected with the indicated relative amounts of gB- or gB$_{C777A}$-coding mRNAs, along with gH pentamer subunits and T7 RNA polymerase mRNAs; the luciferase-reporter fusion assay was carried out as in Fig. 8*B* in the presence (*light gray*) or absence (*dark gray*) of 50 μM 2Br-palmitate. *Error bars* indicate mean ± S.D. *B*, ARPE cells were co-transfected with gH pentamer and the indicated relative amounts of gB- or gB$_{C777A}$-coding mRNAs. Cell nuclei were stained with DAPI; multinucleated cells are indicated by *white arrows*.

Discussion

Cholesterol-rich membrane microdomains play critical roles as self-assembling partitions of specific proteins. Recent advances in this field are demonstrating that raft integral mem-

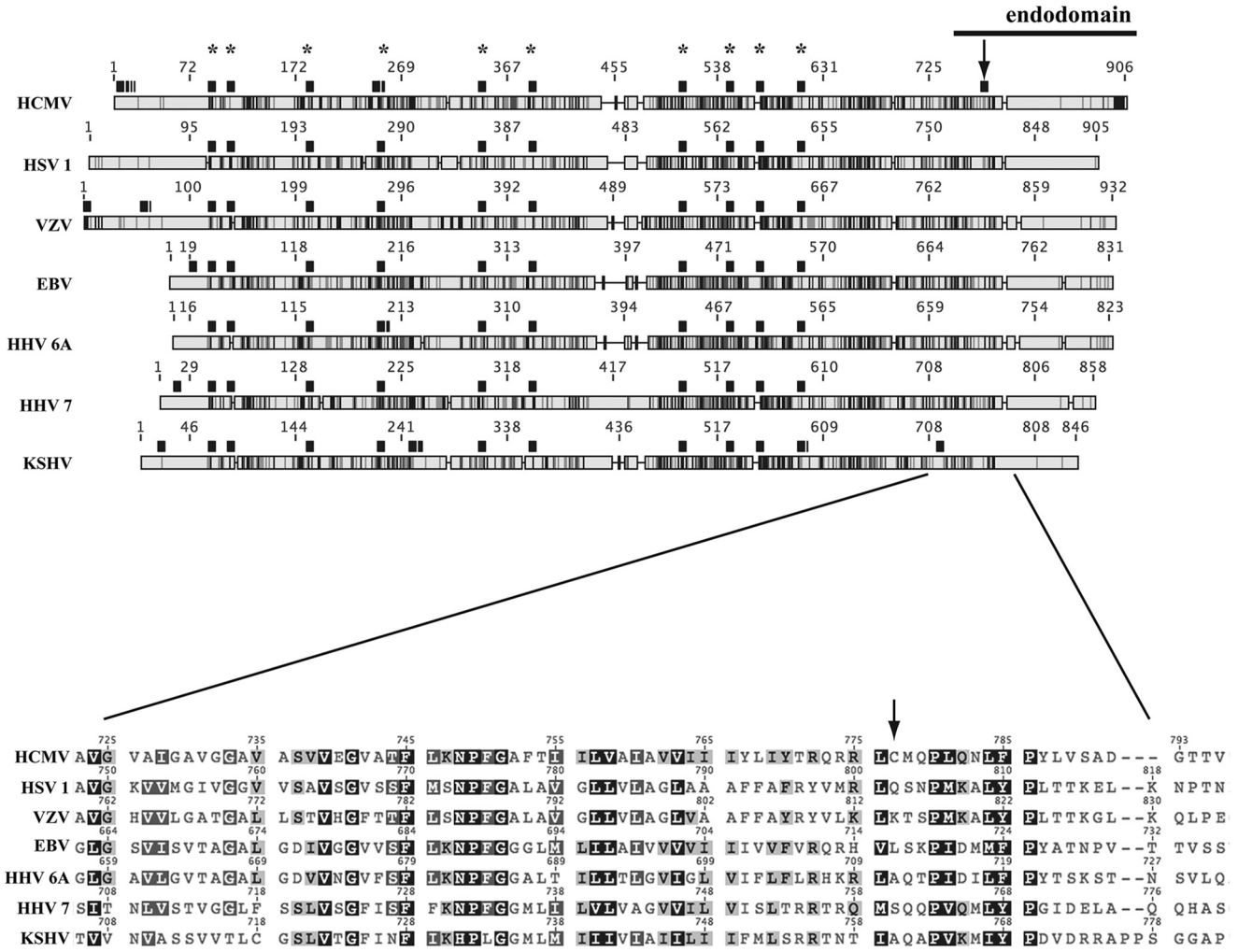

FIGURE 11. **Alignment of gB protein homologs encoded by human herpesviruses.** Overall sequence homology of gB conceptual translation from human herpesviruses (see Footnote 3) is shown schematically in grayscale (*light gray*, no homology; *black*, identity). Cys residues are highlighted with *black squares* above each sequence (*asterisks* mark conserved Cys); *arrow* points to HCMV gB Cys-777. The close-up view shows the alignment in the juxtamembrane-TM region. *VZV*, varicella zoster virus; *HHV 6A*, human herpesvirus 6A; *HHV 7*, human herpesvirus 7; KSHV, Kaposi's sarcoma-associated herpesvirus.

brane proteins (rIMPs), rather than mere cargoes, stabilize the inherently short-lived assembly of cholesterol with companion lipids, by hydrophobic matching with their transmembrane domains (TMs). The raft phases surrounding rIMP TMs are proposed to grow to larger platforms by further supramolecular interactions, often involving protein acylation (33). One pair of cholesterol molecules was shown to pack within the hollow formed by two palmitoyl residues in the groundbreaking x-ray structure of the mono-palmitoylated β_2-adrenergic receptor (34). The cholesterol-palmitic interaction seemed to rely on steric packing only. Whether this arrangement in the depth of a non-polar environment could lead to a stable binding was not addressed. Based on data collected in this work, we propose that palmitoylation drives the growth of cholesterol-dependent protein multimers by increasing protein-cholesterol friction. We showed that HCMV gB features the intrinsic ability to localize into cholesterol-dependent microdomains and that the newly discovered palmitoylated Cys-777 considerably enhances a basal, low-grade gB partition (Figs. 1–5). The multimerization analysis of purified gB demonstrated that the residence time of cholesterol within multimers is palmitoylation-dependent (Figs. 6 and 7) and correlates with multimer stability, although it does not support a role for acylation in cholesterol-gB stable binding. Further work is needed to clarify whether gB TM protein backbone actually holds any cholesterol site. Notably, our results are reminiscent of the high occupancy site hypothesis raised from molecular simulations of G protein-coupled receptor-cholesterol interactions (35), in which it is suggested that cholesterol-protein interactions are highly dynamic and that they swiftly exchange between adjacent cholesterol sites. The clustering model by high exchange rate under limited interactor diffusion, proposed by Woolf and Linderman (36), explains the stability of gB multimers by cholesterol diffusion confinement. It is plausible that this phenomenon is strengthened by the three-fold symmetry of the gB monomer, and we suggest that palmitoylation generates cholesterol hot-spots between gB monomers. In turn, this may build a defined layer where cholesterol from the target cell membrane and the virion envelope can mix. Indeed, gB raft localization and clustering have been so far shown to be related to virion entry and post-fusion gB (19, 20), and our experiments on multimerization also made use of post-fusion full-length gB, as characterized by electron micros-

copy (21). The gB moiety, C-terminal to the ectodomain, displayed a compact fold in EM two-dimensional reconstructions. However, it is yet unknown whether pre- and post-fusion gB conformations differ in the relative orientation of TM helices or in their interaction with cholesterol. At the same time, ectopically expressed gB associates with the raft phase in both insect and human cells, independently from fusion triggers.

The evidence that inhibition of protein palmitoylation and palmitoylation site mutagenesis both impaired gB fusion activity in human epithelial cells (Figs. 8–10) is significant. These data reinforce the idea that the clustering of virion fusogens provides both the mechanical force and the energy required for the pore formation.

The chance to observe a diffusivity effect in cholesterol-gB multimers makes the point for an interesting speculation about the energetics in virion-mediated membrane fusion. Under mechanical stress, viscous substances release heat as the consequence of internal forces. It is conceivable that the deformation in the hemifused membranes around the refolded gB multimers cooperates with the ectodomain in supplying the energy needed to the pore formation (see Ref. 37 for the correlations in membrane deformation, bending heat, and melting). This hypothesis is supported by the observed binding to the liquid order/disorder inter-phase by the HIV gp41 fusogenic peptide (38).

Palmitoylation also affects gB trafficking at the plasma membrane. Although this is likely not relevant *per se* in HCMV virogenesis (39), the data reinforce the idea that the supramolecular organization of rIMPs impacts membrane dynamics. Moreover, the virion assembly compartment observed in cells infected by herpesviruses shares similarities with the multivesicular body, whose lipid bilayer is contributed by the plasma membrane. Hence, the relationships that gB has with cell surface lipids could also occur during nucleocapsid envelopment at the end of the virus assembly process. In this view, the interplay of gB with the other two known HCMV palmitoylated proteins, gN and pp28, both linked to virogenesis (40), may deserve deeper investigation in the near future.

Intriguingly, gB palmitoylation seems to be specific to HCMV among herpesviruses, because only this species codes for a Cys residue in the endodomain of the fusion protein (Fig. 11). Elucidating the outcome of such a divergence will shed light on the supramolecular level of herpesviral fusion machineries. The question of whether evolving a palmitoylation site has added new features to HCMV gB, or whether non-HCMV gB TMs can provide analogous cholesterol hot-spots without *S*-acylation, is fascinating.

Finally and (to some extent) independently from the role that gB multimerization plays in the infection cycle, antigen clustering is a powerful tool in synthetic vaccinology for boosting an immune response. Along with artificial adjuvants, multimerization determinants can be exploited to push the efficacy of subunit vaccine candidates protecting against herpesviral infections.

Author Contributions—M. P., A. S. C., A. P. T., and P. M. A. conceived the study, analyzed the data and wrote the paper. M. P. designed, performed and analyzed the experiments.

Acknowledgments—We thank Didier Trono for pMDLg/pRRE plasmid, Andrea Carfi for inspiring discussion, Piergiuseppe Nestola for the guidance with NTA, Giorgio Gribaudo for the ARPE19 cell line, and Franca Rossi for the critical reading of the manuscript.

References

1. Davison, A. J., Eberle, R., Ehlers, B., Hayward, G. S., McGeoch, D. J., Minson, A. C., Pellett, P. E., Roizman, B., Studdert, M. J., and Thiry, E. (2009) The order Herpesvirales. *Arch. Virol.* **154,** 171–177
2. Sinzger, C., Digel, M., and Jahn, G. (2008) Cytomegalovirus cell tropism. *Curr. Top. Microbiol. Immunol.* **325,** 63–83
3. Britt, W. (2008) Manifestations of human cytomegalovirus infection: proposed mechanisms of acute and chronic disease. *Curr. Top. Microbiol. Immunol.* **325,** 417–470
4. Fülöp, T., Larbi, A., and Pawelec, G. (2013) Human T cell aging and the impact of persistent viral infections. *Front. Immunol.* **4,** 271
5. Heldwein, E. E. (2009) Entry of herpesviruses into cells: more than one way to pull the trigger. *Structure* **17,** 147–149
6. Hahn, G., Revello, M. G., Patrone, M., Percivalle, E., Campanini, G., Sarasini, A., Wagner, M., Gallina, A., Milanesi, G., Koszinowski, U., Baldanti, F., and Gerna, G. (2004) Human cytomegalovirus UL131–128 genes are indispensable for virus growth in endothelial cells and virus transfer to leukocytes. *J. Virol.* **78,** 10023–10033
7. Patrone, M., Secchi, M., Fiorina, L., Ierardi, M., Milanesi, G., and Gallina, A. (2005) Human cytomegalovirus UL130 protein promotes endothelial cell infection through a producer cell modification of the virion. *J. Virol.* **79,** 8361–8373
8. Wang, D., and Shenk, T. (2005) Human cytomegalovirus virion protein complex required for epithelial and endothelial cell tropism. *Proc. Natl. Acad. Sci. U.S.A.* **102,** 18153–18158
9. Vanarsdall, A. L., and Johnson, D. C. (2012) Human cytomegalovirus entry into cells. *Curr. Opin. Virol.* **2,** 37–42
10. Krummenacher, C., Carfí, A., Eisenberg, R. J., and Cohen, G. H. (2013) Entry of herpesviruses into cells: the enigma variations. *Adv. Exp. Med. Biol.* **790,** 178–195
11. Patrone, M., Secchi, M., Bonaparte, E., Milanesi, G., and Gallina, A. (2007) Cytomegalovirus UL131–128 products promote gB conformational transition and gB-gH interaction during entry into endothelial cells. *J. Virol.* **81,** 11479–11488
12. Atanasiu, D., Saw, W. T., Cohen, G. H., and Eisenberg, R. J. (2010) Cascade of events governing cell-cell fusion induced by herpes simplex virus glycoproteins gD, gH/gL, and gB. *J. Virol.* **84,** 12292–12299
13. Harrison, S. C. (2008) Viral membrane fusion. *Nat. Struct. Mol. Biol.* **15,** 690–698
14. Heldwein, E. E., Lou, H., Bender, F. C., Cohen, G. H., Eisenberg, R. J., and Harrison, S. C. (2006) Crystal structure of glycoprotein B from herpes simplex virus 1. *Science* **313,** 217–220
15. Hannah, B. P., Heldwein, E. E., Bender, F. C., Cohen, G. H., and Eisenberg, R. J. (2007) Mutational evidence of internal fusion loops in herpes simplex virus glycoprotein B. *J. Virol.* **81,** 4858–4865
16. Sharma, S., Wisner, T. W., Johnson, D. C., and Heldwein, E. E. (2013) HCMV gB shares structural and functional properties with gB proteins from other herpesviruses. *Virology* **435,** 239–249
17. Bentz, J. (2000) Minimal aggregate size and minimal fusion unit for the first fusion pore of influenza hemagglutinin-mediated membrane fusion. *Biophys. J.* **78,** 227–245
18. Key, T., and Duncan, R. (2014) A compact, multifunctional fusion module directs cholesterol-dependent homomultimerization and syncytiogenic efficiency of reovirus p10 FAST proteins. *PLoS Pathog.* **10,** e1004023
19. Maurer, U. E., Zeev-Ben-Mordehai, T., Pandurangan, A. P., Cairns, T. M., Hannah, B. P., Whitbeck, J. C., Eisenberg, R. J., Cohen, G. H., Topf, M., Huiskonen, J. T., and Grünewald, K. (2013) The structure of herpesvirus fusion glycoprotein B-bilayer complex reveals the protein-membrane and lateral protein-protein interaction. *Structure* **21,** 1396–1405
20. Bender, F. C., Whitbeck, J. C., Ponce de Leon, M., Lou, H., Eisenberg, R. J., and Cohen, G. H. (2003) Specific association of glycoprotein B with lipid

rafts during herpes simplex virus entry. *J. Virol.* **77,** 9542–9552
21. Patrone, M., Carinhas, N., Sousa, M. Q., Peixoto, C., Ciferri, C., Carfi, A., and Alves, P. M. (2014) Enhanced expression of full-length human cytomegalovirus fusion protein in non-swelling baculovirus-infected cells with a minimal fed-batch strategy. *PLoS ONE* **9,** e90753
22. Dull, T., Zufferey, R., Kelly, M., Mandel, R. J., Nguyen, M., Trono, D., and Naldini, L. (1998) A third-generation lentivirus vector with a conditional packaging system. *J. Virol.* **72,** 8463–8471
23. Carmo, M., Dias, J. D., Panet, A., Coroadinha, A. S., Carrondo, M. J., Alves, P. M., and Cruz, P. E. (2009) Thermosensitivity of the reverse transcription process as an inactivation mechanism of lentiviral vectors. *Hum. Gene Ther.* **20,** 1168–1176
24. Drisdel, R. C., and Green, W. N. (2004) Labeling and quantifying sites of protein palmitoylation. *BioTechniques* **36,** 276–285
25. Brigidi, G. S., and Bamji, S. X. (2013) Detection of protein palmitoylation in cultured hippocampal neurons by immunoprecipitation and acyl-biotin exchange (ABE). *J. Vis. Exp.* **72,** 50031
26. Persaud-Sawin, D. A., Lightcap, S., and Harry, G. J. (2009) Isolation of rafts from mouse brain tissue by a detergent-free method. *J. Lipid Res.* **50,** 759–767
27. Schindler, J., and Nothwang, H. G. (2006) Aqueous polymer two-phase systems: effective tools for plasma membrane proteomics. *Proteomics* **6,** 5409–5417
28. Waheed, A. A., and Freed, E. O. (2010) The role of lipids in retrovirus replication. *Viruses* **2,** 1146–1180
29. Gheysen, D., Jacobs, E., de Foresta, F., Thiriart, C., Francotte, M., Thines, D., and De Wilde, M. (1989) Assembly and release of HIV-1 precursor $Pr55^{gag}$ virus-like particles from recombinant baculovirus-infected insect cells. *Cell* **59,** 103–112
30. Veit, M. (2012) Palmitoylation of virus proteins. *Biol. Cell* **104,** 493–515
31. Yang, W., Di Vizio, D., Kirchner, M., Steen, H., and Freeman, M. R. (2010) Proteome scale characterization of human *S*-acylated proteins in lipid raft-enriched and non-raft membranes. *Mol. Cell. Proteomics* **9,** 54–70
32. Levental, I., Lingwood, D., Grzybek, M., Coskun, U., and Simons, K. (2010) Palmitoylation regulates raft affinity for the majority of integral raft proteins. *Proc. Natl. Acad. Sci. U.S.A.* **107,** 22050–22054
33. Simons, K., and Gerl, M. J. (2010) Revitalizing membrane rafts: new tools and insights. *Nat. Rev. Mol. Cell Biol.* **11,** 688–699
34. Cherezov, V., Rosenbaum, D. M., Hanson, M. A., Rasmussen, S. G., Thian, F. S., Kobilka, T. S., Choi, H. J., Kuhn, P., Weis, W. I., Kobilka, B. K., and Stevens, R. C. (2007) High-resolution crystal structure of an engineered human β_2-adrenergic G protein-coupled receptor. *Science* **318,** 1258–1265
35. Sengupta, D., and Chattopadhyay, A. (2015) Molecular dynamics simulations of GPCR-cholesterol interaction: an emerging paradigm. *Biochim. Biophys. Acta* **1848,** 1775–1782
36. Woolf, P. J., and Linderman, J. J. (2003) Self organization of membrane proteins via dimerization. *Biophys. Chem.* **104,** 217–227
37. Heimburg, T. (2003) Coupling of chain melting and bilayer structure: domains, rafts, elasticity and fusion. in *Planar Lipid Bilayers (BLM's) and Their Applications* (Tien, H. T., and Ottova-Leitmannova, A., eds), pp. 269–293, Elsevier, Heidelberg
38. Yang, S. T., Kiessling, V., Simmons, J. A., White, J. M., and Tamm, L. K. (2015) HIV gp41-mediated membrane fusion occurs at edges of cholesterol-rich lipid domains. *Nat. Chem. Biol.* **11,** 424–431
39. Jarvis, M. A., Fish, K. N., Soderberg-Naucler, C., Streblow, D. N., Meyers, H. L., Thomas, G., and Nelson, J. A. (2002) Retrieval of human cytomegalovirus glycoprotein B from cell surface is not required for virus envelopment in astrocytoma cells. *J. Virol.* **76,** 5147–5155
40. Mach, M., Osinski, K., Kropff, B., Schloetzer-Schrehardt, U., Krzyzaniak, M., and Britt, W. (2007) The carboxy-terminal domain of glycoprotein N of human cytomegalovirus is required for virion morphogenesis. *J. Virol.* **81,** 5212–5224